Construction of three-dimensional extrusion limit diagram for magnesium alloy using artificial neural network and its validation

Bai, Shengwen; Fang, Gang; Zhou, Jie

DOI
10.1016/j.jmatprotec.2019.116361

Publication date
2020

Document Version
Accepted author manuscript

Published in
Journal of Materials Processing Technology

Citation (APA)
Bai, S., Fang, G., & Zhou, J. (2020). Construction of three-dimensional extrusion limit diagram for magnesium alloy using artificial neural network and its validation. *Journal of Materials Processing Technology*, *275*, Article 116361. https://doi.org/10.1016/j.jmatprotec.2019.116361

Construction of three-dimensional extrusion limit diagram for magnesium alloy using artificial neural network and its validation

Shengwen Bai[1], Gang Fang[1,*], Jie Zhou [2]

[1] State Key Laboratory of Tribology, Department of Mechanical Engineering, Tsinghua University, Beijing 100084, China

[2] Department of Biomechanical Engineering, Delft University of Technology, Mekelweg 2, 2628 CD Delft, The Netherlands

*Corresponding author, Gang Fang: Tel: +86-10-6278 2694, E-mail: fangg@tsinghua.edu.cn

Abstract

Conventional extrusion limit diagram (ELD) involves only two extrusion process variables and as such it does not account for the combined effects of multiple process parameters on the extrusion process with respect to pressure requirement and extrudate temperature. Attempts were made in the present research to construct three-dimensional (3D) ELD for a magnesium alloy in the space of initial billet temperature, extrusion ratio and extrusion speed. A method to build 3D ELD by integrating finite element (FE) simulations, extrusion experiments and artificial neural networks (ANN) was developed. In addition to initial billet temperature, extrusion ratio and extrusion speed, the temperature difference between the extrusion tooling and billet, the size of the billet and the shape complexity of the extrudate were taken

as the additional process variables and integrated into the equivalent initial billet temperature, extrusion ratio and extrusion speed. The FE simulations, verified by performing extrusion experiments to produce magnesium alloy rods, were used to generate datasets for training the ANN. The ANN then predicted the peak values of extrusion pressure and extrudate temperature over a wider range of extrusion conditions, based on which a 3D ELD for the magnesium alloy was constructed. The 3D ELD was finally validated by performing extrusion experiments to produce magnesium alloy tubes. The results demonstrated that the constructed 3D ELD was reliable and able to provide guidelines for the selection of appropriate extrusion conditions.

Keywords: Magnesium; Extrusion; Extrusion limit diagram; Hot shortness; Artificial neural networks.

1. Introduction

Hot extrusion, mostly applied to aluminum alloys, is a predominant metal-forming process to produce long profiles with unvaried cross sections. With ever increasing demands for light-weight profiles in ground vehicles in recent years, more and more attention has been paid to the extrusion of magnesium alloys. It has been widely recognized that the extrusion of magnesium alloys is not as easy as the extrusion of aluminum alloys and defects are more prone to occur, when the temperature of the extrudate at the die exit exceeds a certain value. At a high initial billet temperature,

the extrudate temperature easily reaches the incipient melting points of magnesium alloys, subsequently resulting in the occurrence of hot shortness on the extrudate surface (Luo et al., 2011). On the other hand, if a low initial billet temperature is employed, there is a risk of excessive extrusion pressure requirement, which may exceed the pressure capacity of the extrusion press used (Barnett et al., 2003). In addition, both applicable extrusion speed and extrusion ratio are limited by the risks of hot shortness and excessive extrusion pressure requirement, leading to low productivity of magnesium alloy extrusion (Zeng et al., 2019). Therefore, the main extrusion process variables, i.e., initial billet temperature, extrusion ratio and extrusion speed, have to be carefully chosen in order to produce defect-free magnesium alloy profiles and at the same time maximize the productivity.

Extrusion limit diagram (ELD) graphically defines a workable area (i.e., the process window) for an extrusion process, to provide guidelines for the choice of extrusion parameters. It has been applied to the aluminum extrusion process (Tutcher and Sheppard, 1980). ELD is actually an *x*-*y* plot; extrusion speed or extrusion ratio, or their combination expressed as strain rate, is plotted against initial billet temperature. Critical initial billet temperatures and critical extrusion speeds, or extrusion ratios or strain rates, are defined by two limit lines, at which defect, typically hot shortness, is onset and the pressure requirement exceeds the pressure capacity limit of the extrusion press, as shown in Fig. 1 (Jackson and Sheppard, 1997).

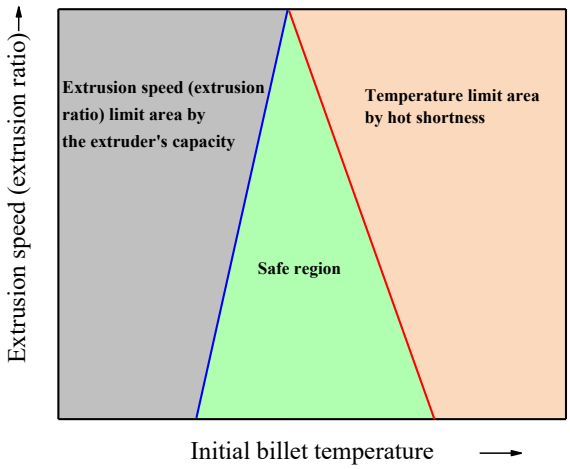

Fig. 1. Schematic of the ELD in the space of extrusion speed (or extrusion ratio) and initial billet temperature.

In the early days, ELD (Sheppard, 1981) was constructed by using two empirical models to define the limits of extrusion pressure and the surface quality of the extrudate. Later on, Clade and Sheppard (1993) added the contour maps of subgrain sizes and surface roughness to the ELD to depict the influence of extrusion condition on the surface quality and microstructural features of the extrudate. Based on the results obtained from extrusion experiments and numerical simulations, Kim et al. (2007) built ELDs and investigated the effect of scandium addition on the extrudability of the 7075 aluminum alloy. The results showed that hot shortness occurred more easily to the alloy with a higher scandium content. In addition to aluminum alloys, ELD was also constructed to determine suitable extrusion parameters for other alloys. For example, Sun et al. (2017) constructed an ELD for the superalloy Inconel 600 with a high nickel content, based on hot processing map.

A number of researchers have extended the application of ELD to magnesium alloy extrusion. Barnett et al. (2003), for example, developed two empirical models to

predict extrusion pressure and extrudate temperature separately and established the ELDs for the extrusion of Mg-Al-Zn alloys. Comparison between the ELDs for magnesium alloys with different Al contents showed that with increasing Al content, the extrusion process window of permissible process parameters shrank. Liu et al. (2008a) also constructed an ELD for the AZ31 magnesium alloy, based on numerical simulations. In their study, initial billet temperature was set at 450 °C so as to leave a sufficient margin for extrudate temperature to rise during extrusion to a point still below the incipient melting point of the alloy at 532 °C. Wang et al. (2007) compared the extrudabilities of the AZ31 and AM30 alloys, according to the ELDs and extrusion experiment results, and found that the extrudability of the AM30 alloy was higher than that of the AZ31 alloy with respect to extrusion pressure requirement and incipient melting temperature.

The construction of ELD requires two functions containing extrusion process parameters to express extrusion pressure requirement and extrudate temperature separately. In the past, empirical models were employed to describe these relationships. Such models had poor generalization performance, mainly because some of the factors, also influencing the extrusion process, were ignored for the sake of simplicity. The need for a more accurate empirical model was recognized, but such an empirical model would involve many parameters and constants and therefore it was not developed for practical use due to its complexity.

Artificial neural networks (ANN) are mathematical systems including interconnected simple neurons that describe complex non-linear relationships between

input and output variables. ANN can learn from the experiences and then predict the new results on the basis of the experience (Li and Bridgwater, 2000). Unlike empirical models, it is not necessary for ANN to consider definite physical significance of parameters, which makes ANN more flexible and convenient for application (Haghdadi et al., 2013). Moreover, ANN have a great ability to handle random data, owing to the readjustment of the weight of each neuron in hidden layer (Yan et al., 2017). In terms of the accuracy of predicted results, ANN are superior to empirical models in many application fields. For example, Yan et al. (2017) used both the ANN and Arrhenius constitutive equation to predict the flow stresses of the Al−6.2Zn−0.70Mg−0.30Mn−0.17Zr alloy during hot compression. The errors of flow stresses predicted from the ANN and Arrhenius constitutive equation were 1.03% and 3.49%, respectively, demonstrating a higher accuracy of the ANN. It was also found that the ANN were superior to the parametric constitutive model to predict the flow stresses of the 7075 aluminum alloy at high strain rates (Sheikh-Ahmad and Twomey, 2007). A neural network system to predict and control springback and maximum strain was developed in a simulated aluminum channel forming process (Cao et al., 2000). The relationship between springback and forming conditions was modeled by the neural network (Ruffini and Cao, 1998). Moreover, the neural network system was superior at minimizing springback when it was compared with the closed-loop control strategy. Owing to the above advantages, ANN have been widely used in many metal-forming processes, including extrusion (Hsiang et al., 2006). Bingöl et al. (2015), for example, used ANN to predict the load for the extrusion of gear-like

profiles. The results showed that the average relative error between the extrusion loads predicted by the ANN and finite element (FE) simulation was only 1.96%. It has been well acknowledged that ANN after training can make reliable predictions of extrusion pressure and extrudate temperature. It suggests that ELD may be constructed by using the results predicted from ANN instead of empirical models.

Conventional ELD is built in the space of extrusion speed versus initial billet temperature, or extrusion ratio versus initial billet temperature. It does not serve the need to reveal the combined effect of extrusion speed and extrusion ratio on the extrusion results. This calls for the construction of ELD in a three-dimensional (3D) coordinate system to reveal the independent and combined effects of initial billet temperature, extrusion ratio and extrusion speed on the extrusion results.

The main objective of the present research was to construct a reliable 3D ELD for a magnesium alloy by using ANN. The results obtained from FE simulations, verified by the extrusion experiments to produce magnesium alloy rods, were used to train ANN. Subsequently, ANN predicted the peak values of extrusion pressure and extrudate temperature at any extrusion conditions, from which a 3D ELD for the magnesium alloy was constructed. Finally, the 3D ELD was validated by the extrusion experiments to produce magnesium alloy tubes.

2. Methodology

To construct 3D ELD, the peak extrusion pressure (P_{peak}) and peak extrudate temperature (T_{peak}) must be expressed as functions of extrusion conditions, namely Eqs. (1) and (2), respectively. The nominal pressure (P_{s}) provided by the extrusion press must be predefined. The critical temperature causing the occurrence of hot shortness (T_{s}) must be determined by performing thermal analysis. The extrusion process reaches its limit, when Eq. (3) or Eq. (4) is satisfied.

$$P_{\mathrm{peak}} = g_1(\text{extrusion conditions}) \tag{1}$$

$$T_{\mathrm{peak}} = g_2(\text{extrusion conditions}) \tag{2}$$

$$P_{\mathrm{peak}} = P_{\mathrm{s}} \tag{3}$$

$$T_{\mathrm{peak}} = T_{\mathrm{s}} \tag{4}$$

Fig. 2 shows the strategy developed in this research to construct 3D ELD for magnesium alloy. Instead of empirical models, ANN was used to describe the relationships between extrusion conditions (input factors) and extrusion results (output factors). The input factors determining the output factors included initial billet temperature (T_{b}), extrusion ratio (r) and extrusion speed (V_{e}). Furthermore, the temperature difference between the die and billet (ΔT_{db}), the shape factor of the cross section of the extrudate (λ), the length of the billet (L) and the inner diameter of the container (D) that also influenced extrusion pressure and extrudate temperature were also taken into consideration. The shape factor (λ) reflecting the shape complexity of the cross section of the extrudate was defined as the ratio of the perimeter of the

actual extrudate cross section to the perimeter of an equivalent circular section of equal cross-section area (Qamar et al., 2004). Obviously, large-scale ANN and a very large number of training datasets would be necessary, if all the seven process parameters mentioned above were taken as the input variables of ANN. Moreover, ELD would be constructed in a multi-dimensional space containing seven axes representing these seven parameters.

For the sake of simplicity, the effects of ΔT_{db}, λ, L and D on the output factors were taken into consideration by using them to modify the three main process parameters, i.e., T_b, r and V_e. The seven parameters were integrated into these three process parameters, namely equivalent initial billet temperature ($\overline{T_b}$), equivalent extrusion ratio ($\bar{r}$) and equivalent extrusion speed ($\overline{V_e}$), as expressed by Eqs. (5)-(7). For example, $\overline{T_b}$ is a function of T_b and ΔT_{db}, representing the initial temperatures of the billet and die. The equivalent extrusion ratio $\bar{r}$ is a parameter that integrates extrusion ratio (r), shape factor (λ) and the dimensions of the billet (L and D). In the present research, the equivalent parameters, $\overline{V_e}$, $\overline{T_b}$ and $\bar{r}$, were employed as the input factors of ANN and the output factors were set to be P_{peak} and T_{peak}.

$$\overline{V_e} = \frac{\bar{r}}{r} V_e \tag{5}$$

$$\overline{T_b} = T_b + f_1(\Delta T_{db}) \tag{6}$$

$$\bar{r} = r f_2(\lambda, L, D) \tag{7}$$

When the parameters ΔT_{db}, λ, L and D were fixed and with the specific values of ΔT_{db}^*, λ^*, L^* and D^*, the equivalent parameters $\overline{V_e}$, $\overline{T_b}$ and $\bar{r}$ were equal to V_e, T_b and r, respectively. The extrusion experiments to produce rods at various conditions

were regarded as simple extrusion, while the extrusion experiments for producing profiles under various conditions were considered complex extrusion. The basic strategy adopted in the present research was to convert complex extrusion into simple extrusion, and then predict the extrusion pressure and extrudate temperature through the ANN. To this end, the following two tasks would have to be completed in order to predict the extrusion pressure and extrudate temperature for any complex extrusion by the ANN: (i) the ANN should be trained with the data drawn from simple extrusion; (ii) the relationship between complex extrusion and simple extrusion should be determined.

Finite element (FE) simulations of simple extrusion, verified by corresponding rod extrusion experiments, were performed at different r, T_b and V_e values to collect datasets to be used to train ANN. After training, the ANN could predict P_{peak} and T_{peak} values of simple extrusion.

The specific expressions of the equivalent parameters $\overline{T_b}$ and $\bar{r}$ (Eqs. (6) and (7)) were determined through non-linear regression on the basis of ANN and FE simulations at different ΔT_{db}, λ, L and D values. By using this method, P_{peak} and T_{peak} values during extrusion to produce any profiles under any conditions could be predicted by using the ANN.

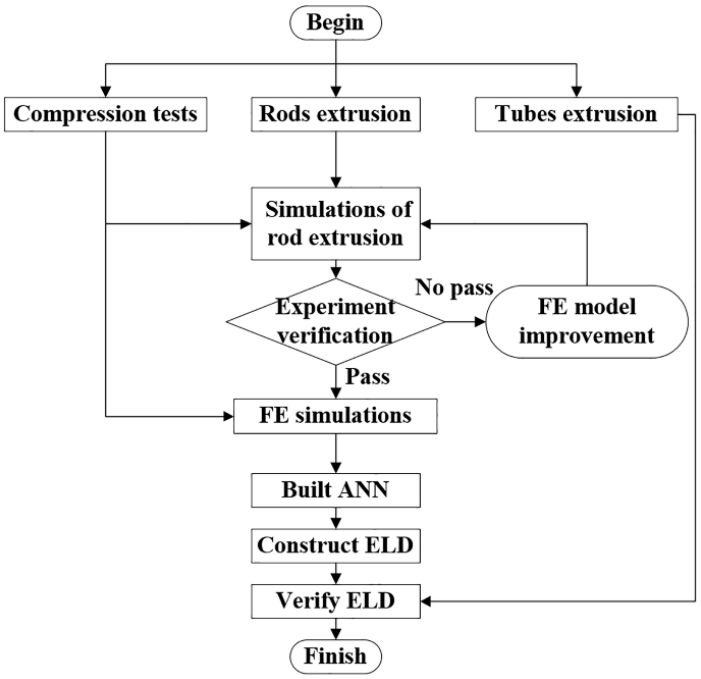

Fig. 2. Flow chart of the construction of 3D ELD for magnesium alloy.

By using the ANN, 3D ELD was then constructed in a three-dimensional coordinate system of $\overline{V_e}$, $\overline{T_b}$ and $\bar{r}$. In fact, the coordinate axes of $\overline{V_e}$, $\overline{T_b}$ and $\bar{r}$ represented the production efficiency, initial heating conditions and deformation degree applied to extrusion. The 3D ELD constructed in the current work was based on the extrusion experiments to produce magnesium alloy rods, as well as FE simulations and ANN. Finally, the extrusion experiments to produce magnesium alloy tubes were carried out to validate the applicability and accuracy of the 3D ELD.

3. Experiments and FE simulations

3.1 Material and compression tests

The magnesium alloy Mg-8Al-0.5Zn-0.5RE containing rare earth elements of La (0.7%-1.3%) and Gd (0.3%-0.7%) was selected as the exemplary test material. The

as-cast alloy was subjected to a solid solution treatment at 420 °C for 24 h before compression tests. According to a previous study (Bai et al., 2019), the temperature limit (T_s) of the present magnesium alloy, corresponding to the occurrence of hot shortness, was 481 °C.

Uniaxial compression tests of cylindrical specimens with a diameter of 8 mm and a height of 12 mm were performed using a thermomechanical simulator (Gleeble 1500D, DSI, USA). Test temperatures were set from 300 to 420 °C with an interval of 30 °C. Strain rates were 0.001, 0.01, 0.1, 1 and 10 s^{-1}. A hyperbolic sine-type equation (Eq. (8)), proposed by Sellars and McTegart (1996), was employed to describe the deformation behavior of the material. The constitutive constants (Table 1) determined through the compression tests were applied in the FE simulations of magnesium alloy extrusion.

$$\dot{\varepsilon} = A[\sinh(\alpha\sigma)]^n \exp\left(\frac{-Q}{RT}\right) \quad (8)$$

Table 1. Constitutive constants of the magnesium alloy Mg-8Al-0.5Zn-0.5RE.

Constitutive constant	A	α	n	Q (kJ/mol)
Value	2.3188×10^{10}	1.721×10^{-2}	4.5164	141.329

3.2 Extrusion experiments to produce rods for the verification of the FE simulations

To verify the results obtained from the FE simulations, extrusion experiments to produce magnesium alloy rods were performed using a hydraulic press with a force capacity of 2 MN. Fig. 3 shows the schematic diagram of the experimental setup. The as-cast magnesium alloy was machined into rods with a diameter of 29 mm and a

length of 23 mm to produce extrusion billets. They were extruded into finer rods with a diameter of 5.5 mm. The inner diameter of the container liner was 30 mm and consequently the extrusion ratio was 29.8. Initial billet temperatures from 250 to 440 ºC and extrusion speeds from 14.3 to 245.6 mm/s were employed. Before the extrusion experiments, the billet, die and container were preheated to the same target temperature by four heating units inserted into the container. Holding time was 15 min. The actual heating temperature at point A was monitored by a thermocouple inserted into the container liner. During extrusion, the extrusion force applied through the stem was measured by a force sensor installed between the press ram and stem (see Fig. 3). In addition, the temperature at the die orifice (i.e., point B) was measured and registered. The detailed experimental conditions were also described in a previously published paper (Bai et al., 2019).

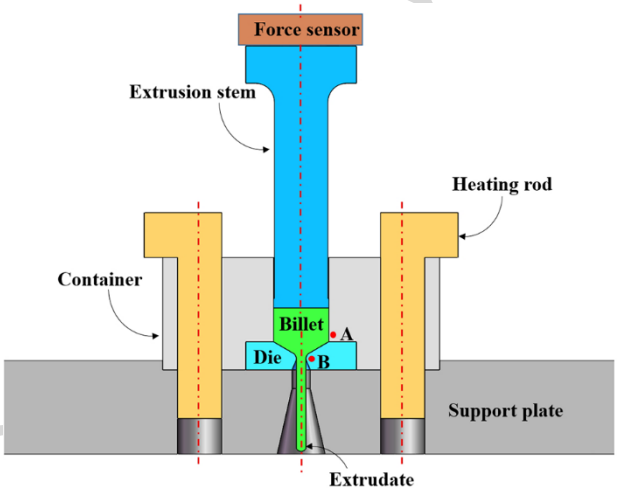

Fig. 3. Schematic diagram of the experimental setup to produce rods.

An essential limiting factor for the extrusion press to run at its full force capacity is the load-bearing capacity of the extrusion tooling. Actually, the lowest value (the yield strength of the stem, the load-bearing capacities of the die and die backer, or the load capacity of the extrusion press) should be taken as the upper limit of extrusion

pressure. If the peak value of extrusion pressure exceeds the yield strength of the stem, the diameter of the stem must be increased, which in turn requires a larger container and results in a larger extrusion ratio for a given extrudate and thus a higher extrusion pressure requirement. In the present research, the yield strength of the stem was taken to be the upper limit of extrusion pressure (P_s). The value was 1360 MPa for the stem made of the tool steel X40CrMoV5-1 (Bauser et al., 2006).

3.3 FE simulations

The FE simulations of extrusion to produce rods were conducted to compare the simulation results with the results obtained from the experiments mentioned in subsection 3.2 and to verify the results obtained from the FE simulations. Details of the simulation work were given in a previous paper (Bai et al., 2019). An axisymmetric model (Fig. 4) was built by using the commercial software package DEFORM. Heat exchanges among all the objects in the model, as well as those between the objects and surrounding environment were taken into consideration. A shear friction model was adopted at the interfaces between the billet and extrusion tooling and the friction factor was set at 1.0 (Li et al., 2008). The constitutive equation of the magnesium alloy (Eq. (8) and Table 1) determined from the hot compression tests were applied in the FE model. The thermal properties of the magnesium alloy and tooling material (H13 tool steel) are listed in Table 2 (Liu et al., 2008b). The initial billet temperatures and extrusion speeds of the FE simulations were the same as those of the extrusion experiments to produce rods.

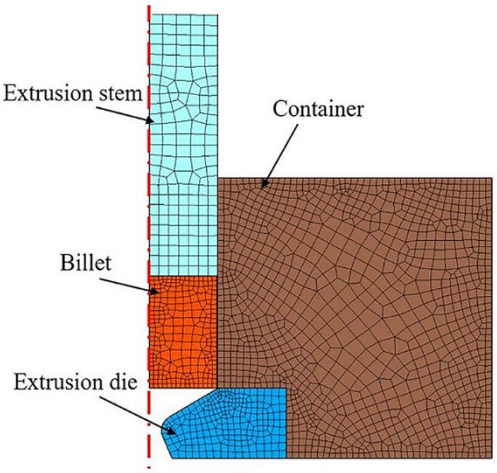

Fig. 4. FE axisymmetric model of the extrusion process to produce rods.

Table 2. Physical properties of the billet and extrusion tooling.

Physical property	Magnesium alloy	H13 tool steel
Thermal conductivity [W/(m °C)]	96	28.4
Heat capacity [N/(mm^2 °C)]	2.097at 327°C 2.275 at 527°C	5.6
Heat transfer coefficient between tooling and workpiece [N/(°C s mm^2)]	11	11
Heat transfer coefficient between tooling/workpiece and air [N/(°C s mm^2)]	0.02	0.02
Emissivity	0.7	0.7

A series of FE simulations of extrusion to produce rods were carried out to prepare datasets for training ANN. As mentioned earlier in Section 2, these FE simulations corresponded to the simple extrusion experiments. In these FE simulations, the temperature difference between the die and billet (ΔT_{db}), the shape factor of the extrudate (λ), the length of the billet (L) and the inner diameter of the container (D) were unchanged, with values of 0 °C, 1, 23 mm and 30 mm, respectively. Moreover,

the input variables of the training dataset, $\overline{V_e}$, $\overline{T_b}$ and $\bar{r}$, were equal to V_e, T_b and r, respectively. Each input variable was set to 6 levels (Table 3), meeting the requirements of the diversity and uniformity of training samples. After the FE simulations, the peak values of extrusion pressure and extrudate temperature were drawn as the output variables of the dataset. Datasets containing 216 samples on basis of these FE simulations were generated.

Table 3. Levels of the parameters used in the FE simulations for preparing ANN training datasets.

Input parameters	Level 1	Level 2	Level 3	Level 4	Level 5	Level 6
$\bar{r}$	5	25	45	65	85	105
$\overline{T_b}$ (°C)	130	200	270	340	410	480
$\overline{V_e}$ (mm/s)	10	90	180	270	360	450

To determine the specific expressions of the equivalent parameters of $\overline{V_e}$, $\overline{T_b}$ and $\bar{r}$ (Eqs. (5)-(7)), FE simulations of extrusion to produce profiles with different values of ΔT_{db}, λ, L and D were carried out. Table 4 shows the variables for the FE simulations. Six profiles with different cross sections were specially designed to create shape factors (λ) values from 1 to 6 (Fig. 5). An extrusion ratio of 45, initial billet temperature of 340 °C and extrusion speed of 150 mm/s were employed in these FE simulations.

Table 4. Variables of the FE simulations for modifying the ELD.

No.	ΔT_{db} (°C)	L (mm)	D (mm)	λ
1	-50, -40, -30, -20, -10, 0, 10, 20, 30, 40, 50	23	30	1
2	0	11.5, 23, 46, 69, 92, 115	30	1
3	0	23	15, 30, 60, 90, 120	1
4	0	140	80	1, 2, 3, 4, 5, 6

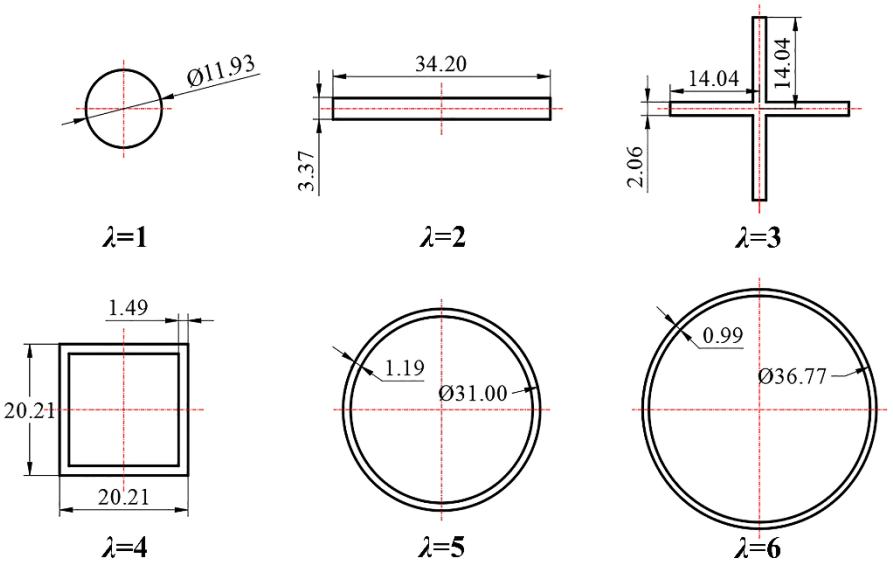

Fig. 5 Cross sections of the profiles with different shape factor λ values.

4. Construction of extrusion limit diagram

4.1 Verification of the FE simulations

The FE simulation results and experimentally measured results at the same extrusion conditions were compared to verify the results obtained from the FE simulations. As an example, the measured and simulated extrusion pressure-stroke curves of the extrusion experiment at an extrusion ratio of 29.8, initial billet temperature of 350 °C and extrusion speed of 117.1 mm/s, are shown in Fig. 6a. The simulated pressure-stroke curve was in good agreement with the measured results. The average difference between the simulated pressure and measured pressure was 6.4%. The peak values of extrusion pressure were of most interest in the present work. Linear regression was used to find the relationship between the peak values of measured and

simulated extrusion pressures at different extrusion conditions (Fig. 6b). The reliability of the FE simulations was thereby confirmed.

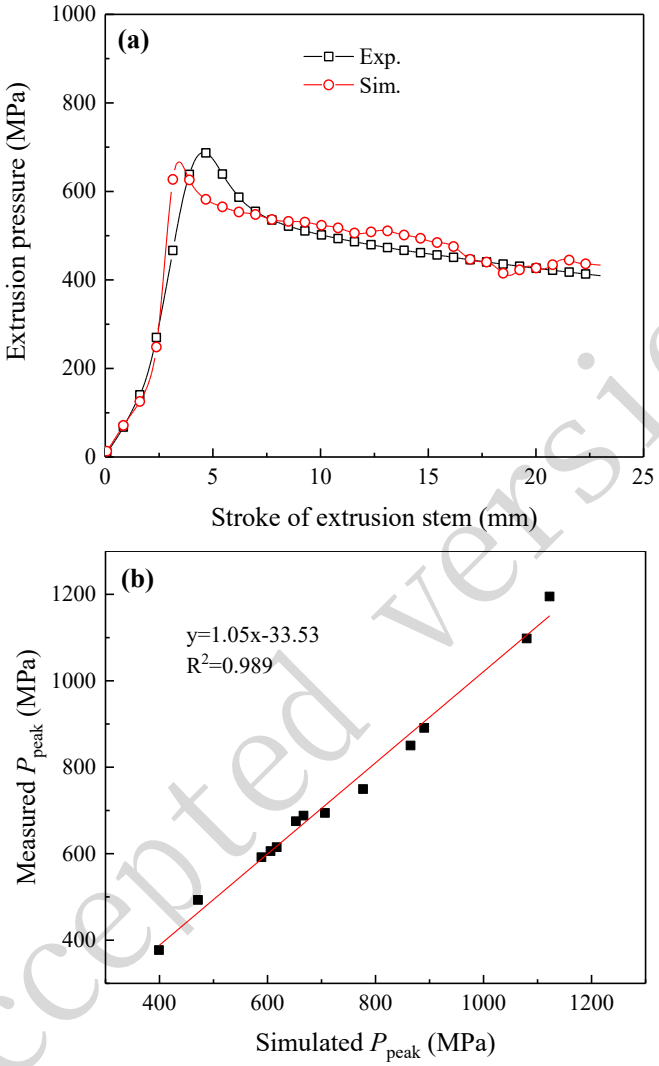

Fig. 6. Comparison between the experimentally measured and simulated extrusion pressures. (a) Extrusion pressure-stroke curves at an extrusion ratio of 29.8, initial billet temperature of 350 °C and extrusion speed of 117.1 mm/s; (b) Linear correlation between the experimental and simulated extrusion pressure values obtained at different extrusion conditions. In the legend, the slop and the correlation coefficient of the fit are given.

The simulated extrudate temperature was also validated through the comparison between the measured and simulated temperatures at point B (Fig. 3) which showed

negligible differences. The comparison was reported in a previously published paper (Bai et al., 2019). This further assured the use of the results from the FE simulations to train ANN for establishing a 3D ELD.

4.2 Training of ANN

ANN describing the relationships between the input variables of $\overline{V_e}$, $\overline{T_b}$ and $\bar{r}$ and the output variables of P_{peak} and T_{peak} were built by using the Neural Network Fitting APP in Matlab. The APP provided a three-layer feed-forward network including input layer, single hidden layer and output layer. The sigmoid function and linear function were employed as the transfer functions of the hidden layer and the output layer, respectively. Hornik et al. (1989) demonstrated that the single hidden layer network containing sufficient neurons had the ability to approximate any complex non-linear relationships between the inputs and outputs. Fig. 7 shows the structure of the ANN. Before training the ANN, both the input variables and output variables should be normalized in the range of 0-1 in order to obtain optimal results and accelerate the convergence (Sola and Sevilla, 1997). Eq. (9) was employed to normalize the training data (Haghdadi et al., 2013),

$$X' = 0.1 + 0.8 \times \left(\frac{X - X_{min}}{X_{max} - X_{min}} \right) \quad (9)$$

where X is the original value, X' is the normalized one corresponding to X, and X_{max} and X_{min} are the maximum and minimum values of a dataset, respectively. 216 cases prepared for the FE simulations were randomly divided into three datasets for training, validating and testing the ANN as the proportions of 70%, 15% and 15%,

respectively.

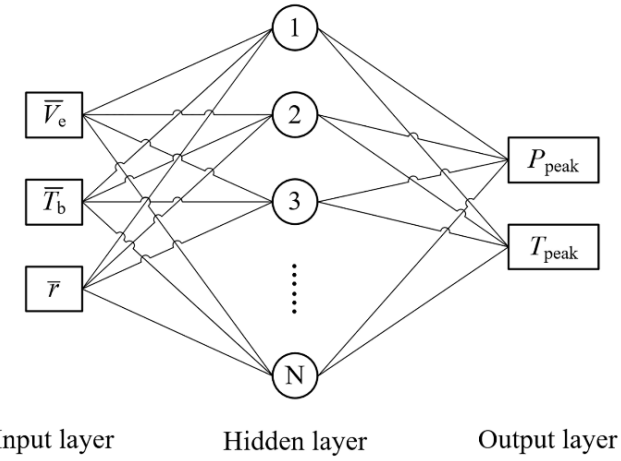

Fig. 7. Structure of the ANN used in the present research.

The proper number of neurons (N) in the hidden layer was determined by combining the method of trial and error with the criterion proposed by Carpenter and Hoffman (1997). According to the criterion, the value of N in the present ANN should be lower than 80 so as to ensure that the ANN could give an overdetermined approximation. Then, the ANN with different N values increased from 3 to 80 were separately trained to obtain the corresponding mean square errors (MSEs) of the test dataset. The computing method for the MSE is shown by Eq. 10, where Y_i and Y_i' are the output variables of the FE simulations and ANN, respectively. The lowest mean square error (MSE) of the test dataset was reached, when the number of neurons in the hidden layer was 20, implying that the ANN had fine generalization performance (Fig. 8). Accordingly, the number of neurons in hidden layer was set to be 20.

$$\mathrm{MSE}=\frac{1}{n}\sum_{i=1}^{n}(Y_i'-Y_i)^2 \tag{10}$$

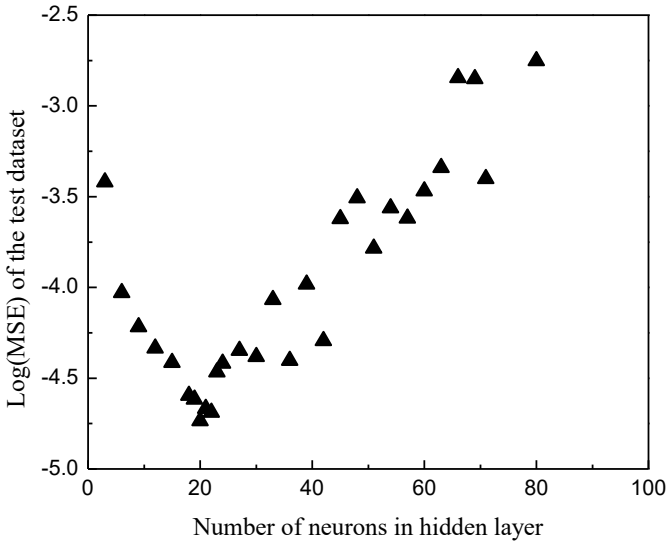

Fig. 8. MSEs of the test dataset calculated by the ANN with different numbers of neurons in the hidden layer.

The normalized testing results of the ANN are shown in Fig. 9. Both the normalized peak values of extrusion pressure and extrudate temperature predicted by the ANN were plotted against those obtained from the FE simulations. The regression lines corresponding to extrusion pressure (Fig. 9 a) and extrudate temperature (Fig. 9 b) had the same slope of 0.998. The R-squares of the two regression lines were 0.9997 and 0.9998, respectively. Both the high R-squares and the regressed lines with the slope close to 1 demonstrated that the results predicted by the ANN were consistent with those from the FE simulations. The ANN established in the present study were hence reliable.

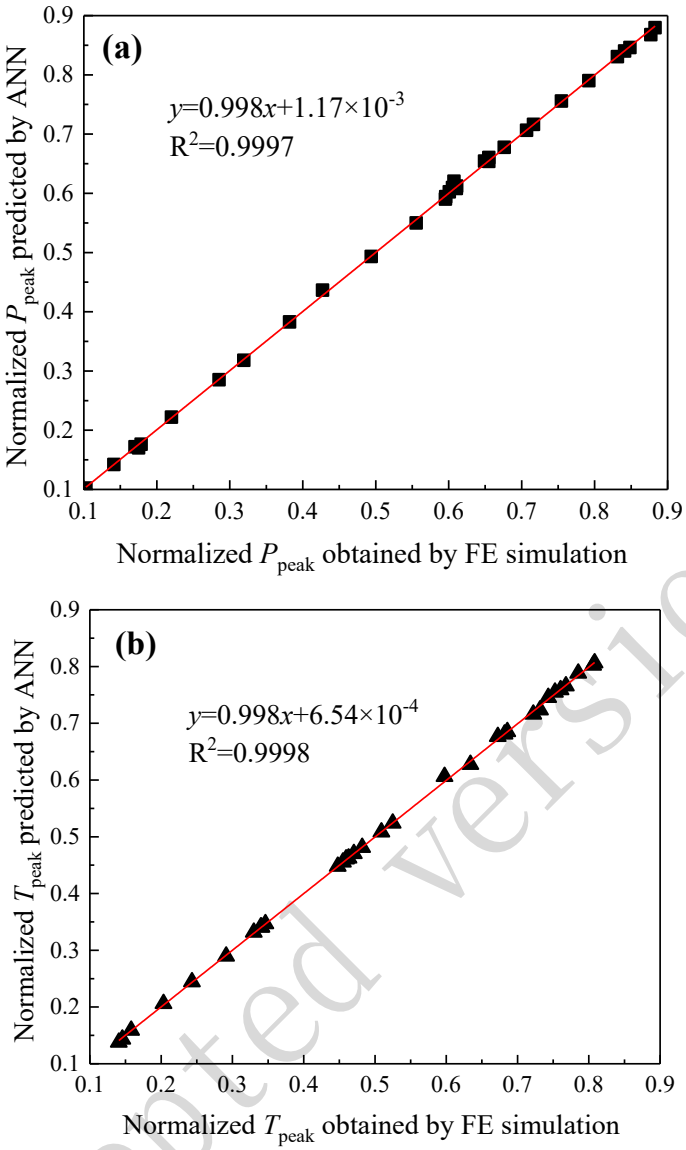

Fig. 9. Extrusion results predicted by the FE simulations and ANN: (a) normalized peak values of extrusion pressure and (b) normalized peak values of extrudate temperature.

To predict the P_{peak} and T_{peak} values during extrusion to produce any profiles by using the ANN, the specific expressions of $\overline{T_b}$ and $\bar{r}$ were determined. Based on the ANN and the simulated P_{peak} and T_{peak} values at different ΔT_{db}, λ, L and D values, the values of the equivalent parameters of $\overline{T_b}$ and $\bar{r}$ were calculated by using the secant method (Ebelechukwu et al., 2018). Then, the expressions of the equivalent parameters were determined by the regression line (Fig. 10). As mentioned in Section 2, $\overline{T_b}$ is a function of T_b and ΔT_{db} (Eq. (6)). Fig. 11a shows a regression curve in the

plot of ΔT_{db} against $\overline{T_b} - T_b$. Eq. (11) is the expression of $\overline{T_b}$. The equivalent extrusion ratio $\bar{r}$ is a function of r, λ, L and D (Eq. (12)), where $f_\lambda(\lambda)$, $f_L(L/L^*)$ and $f_D(D/D^*)$ are separately defined as the influencing factors of λ, L and D. Fig. 11b shows the regression curve in a plot of λ against $f_\lambda(\lambda)$. Eq. (13) describes the relationship between $f_\lambda(\lambda)$ and λ. With the same method, the expressions of $f_L(L/L^*)$ and $f_D(D/D^*)$ were also determined (Eqs. (14) and (15)).

$$\overline{T_b} = T_b + 4.854\left[\frac{\exp(0.095\Delta T_{db})-1}{0.392\exp(0.095\Delta T_{db})+1}\right] \quad (11)$$

$$\bar{r} = r f_\lambda(\lambda) f_L(L/L^*) f_D(D/D^*) \quad (12)$$

$$f_\lambda(\lambda) = 0.785 + 0.215\lambda \quad (13)$$

$$f_L\left(\frac{L}{L^*}\right) = \frac{1.513}{1+1.355\exp(-0.979L/L^*)} \quad (14)$$

$$f_D\left(\frac{D}{D^*}\right) = \frac{0.702}{1-0.997\exp(-1.169D/D^*)} \quad (15)$$

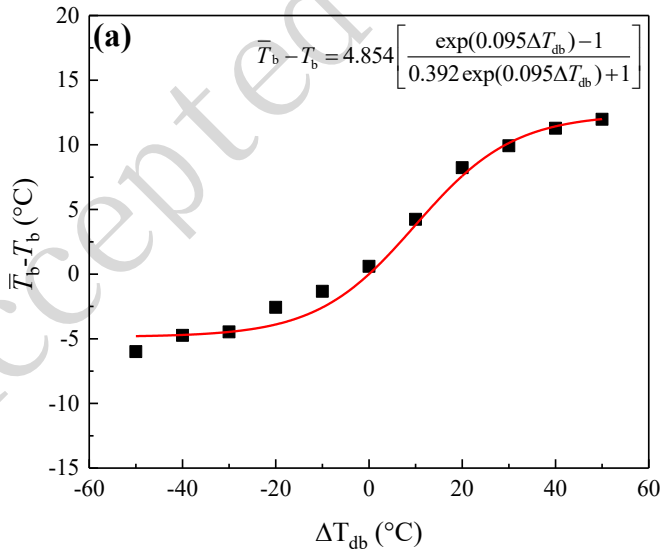

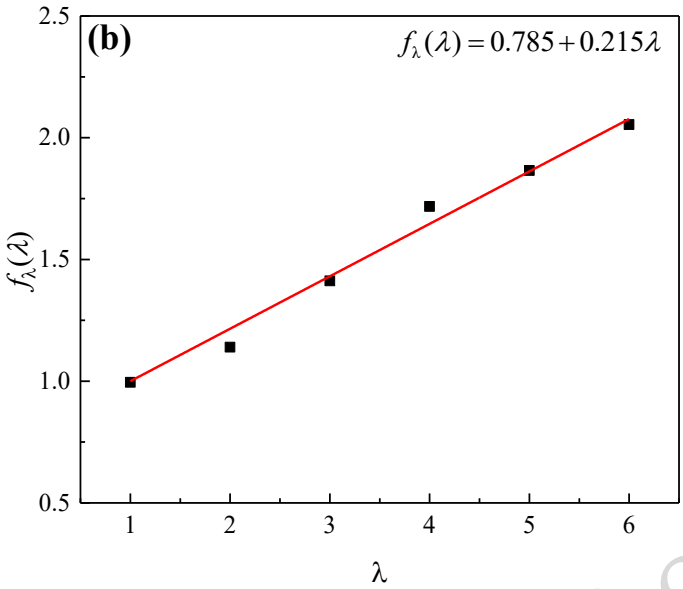

Fig. 10. (a) Regression curve of $\overline{T_b} - T_b$ and (b) influence factor $f_\lambda(\lambda)$.

The ANN built above had great accuracy and generalization performance. It could thus be used to describe the relationships between the input variables and output variables for extrusion to produce any magnesium alloy profiles.

4.3 Establishment of the 3D ELD

As aforementioned, two functions separately linking P_{peak} and T_{peak} with extrusion process parameters are required when an ELD is to be constructed. Based on the FE simulation results, the ANN were built to describe the relationships between the output variables and extrusion process parameters. Eqs. (16) and (17) give the mathematical expressions of the limits of extrusion pressure and billet temperature. Through solving the equations by the secant method (Ebelechukwu et al., 2018), the maximum values of allowable equivalent extrusion speeds ($\overline{V_e}$) at different equivalent parameters of $\overline{T_b}$ and $\bar{r}$ were calculated. Thereafter, the ELD (Fig. 11) of the

magnesium alloy was plotted in a three-dimensional coordinate system, where $\overline{T_b}$, $\bar{r}$ and $\overline{V_e}$ were denoted to be the *x*, *y* and *z* axes, respectively.

$$P_{peak} = \mathrm{ANN_P}(\overline{T_b}, \bar{r}, \overline{V_e}) = P_s \quad (16)$$

$$T_{peak} = \mathrm{ANN_T}(\overline{T_b}, \bar{r}, \overline{V_e}) = T_s \quad (17)$$

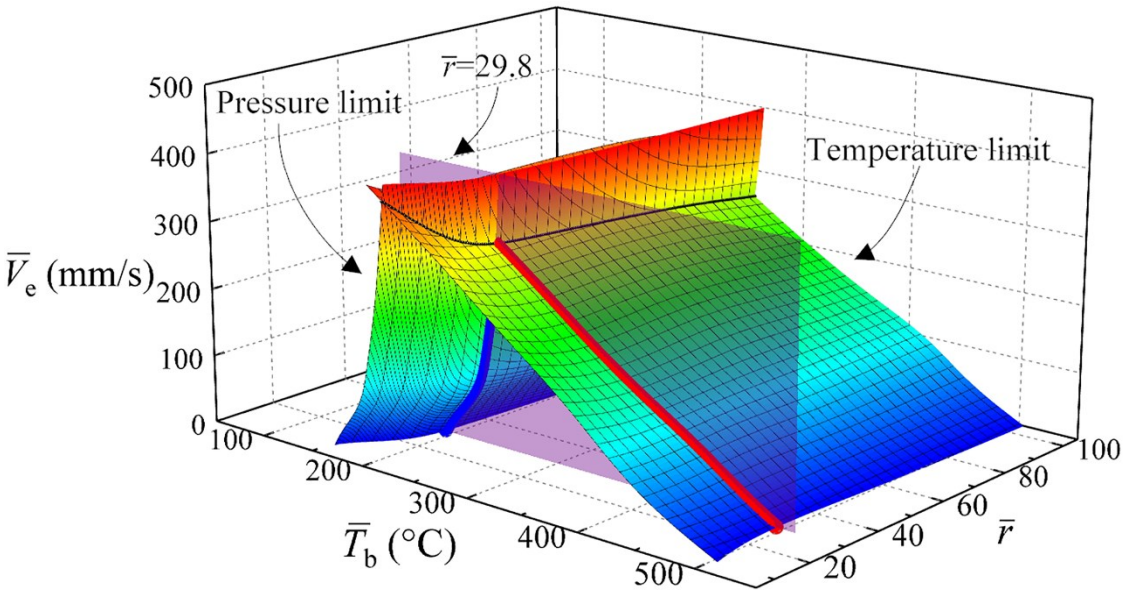

Fig. 11. 3D ELD for the magnesium alloy.

The 3D ELD defined a safe space of the extrusion process parameters by the surfaces representing the extrusion pressure limit and billet temperature limit. It is like a tent, being safe inside and unsafe outside. In the space to the left side of the pressure limit surface, the extrusion pressure will exceed the allowable yield strength of the stem; if the extrusion parameters in this space are chosen, failure of the stem will surely occur due to a too high extrusion pressure. On the other hand, in the space to the right side of the pressure limit, the magnesium alloy can be extruded without the risk of stem failure. In Fig. 11, the temperature limit surface divides the extrusion parameters space into two parts: in the space to the right side of the temperature limit,

hot shortness on the extrudate will appear, because the extrudate temperature will exceed the critical value corresponding to the incipient melting point of the magnesium alloy, while the extrusion with the parameters in the left space will lead to sound extrudate without surface defects. The intersecting curve of the pressure limit surface and temperature limit surface determines the maximum equivalent extrusion speeds at different extrusion ratios. With increasing the equivalent extrusion ratio from 5 to 105, the maximum equivalent extrusion speed decreases from 391 to 259 mm/s.

Compared with conventional ELD constructed in a 2D plane of extrusion speed (extrusion ratio) and initial billet temperature, the present 3D ELD directly reflects the extrudability of the magnesium alloy. For a conventional 2D ELD in a coordinate system of extrusion speed and initial billet temperature, other extrusion process parameters, such as r, ΔT_{db}, λ, L and D are all fixed. As a result, the 2D ELD is only applicable to the extrusion to produce a specific profile. The present 3D ELD is however established for a specific billet material, instead of a specific profile. It can determine the safe extrusion parameters to produce profiles of any cross sections, from simple to complex. The application of the present 3D ELD for a specific extrusion process is run by following four steps:

Step 1: the equivalent extrusion ratio $\bar{r}$ is calculated;

Step 2: the equivalent 2D ELD in the $\overline{V_e}$-$\overline{T_b}$ plane is obtained through intersecting the 3D ELD by the plane of $\bar{r}$;

Step 3: the equivalent 2D ELD is converted into the 2D ELD for a specific profile in the V_e-T_b plane by using Eqs. (5), (11) and (12);

Step 4: the safe extrusion parameters are determined on the basis of the ELD.

For example, the equivalent parameters $\overline{T_b}$, $\bar{r}$ and $\overline{V_e}$ are equal to T_b, r and V_e, respectively, for the standard extrusion experiments to produce magnesium alloy rods. The 2D ELD for these profiles can be directly obtained by intersecting the 3D ELD using the plane at a given extrusion ratio of 29.8, as shown in Fig. 11. The intersected 2D ELD is shown in Fig. 12. The solid circular marks to the right side of the temperature limit line represent the conditions where hot shortness occurs during extrusion. The farther a combination of initial billet temperature and extrusion speed is from the temperature limit line, the more serious hot shortness will be. As shown in Figs. 13, severe hot shortness indeed occurred at the extrusion conditions with the combinations of these two process parameters, namely a: 350 ºC and 245.6 mm/s, d: 400 ºC and 190.4 mm/s and f: 440 ºC and 117. 1 mm/s. However, the other combinations of these two process parameters, such as b: 350 ºC and 190.4 mm/s and e: 400 ºC and 117.1 mm/s, only slight cracks were observed on the surfaces of extruded rods (Fig. 13).

The hollow circular marks inside the process window, such as at point c: 350 ºC and 117.1 mm/s and point g: 440 ºC and 14.3 mm/s, represent the extrusion conditions, at which magnesium rods can be extruded without the occurrence of hot shortness or excessive extrusion pressure requirement. The comparison between Figs. 12 and 13

confirms that the ELD constructed by the ANN can reliably predict the results of extrusion to produce magnesium alloy rods.

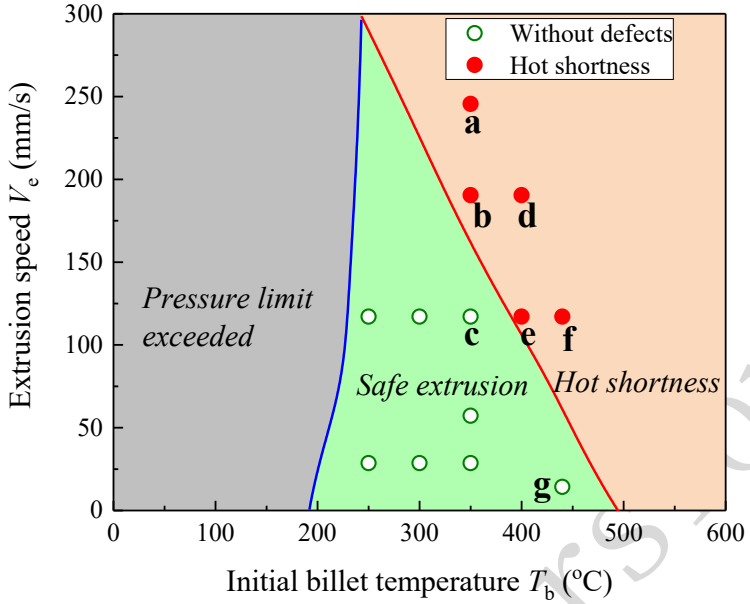

Fig. 12. 2D ELD for the production of magnesium alloy rods at an extrusion ratio of 29.8. The extrudate surfaces under the extrusion conditions marked by the symbols from a to g are shown in Fig.13.

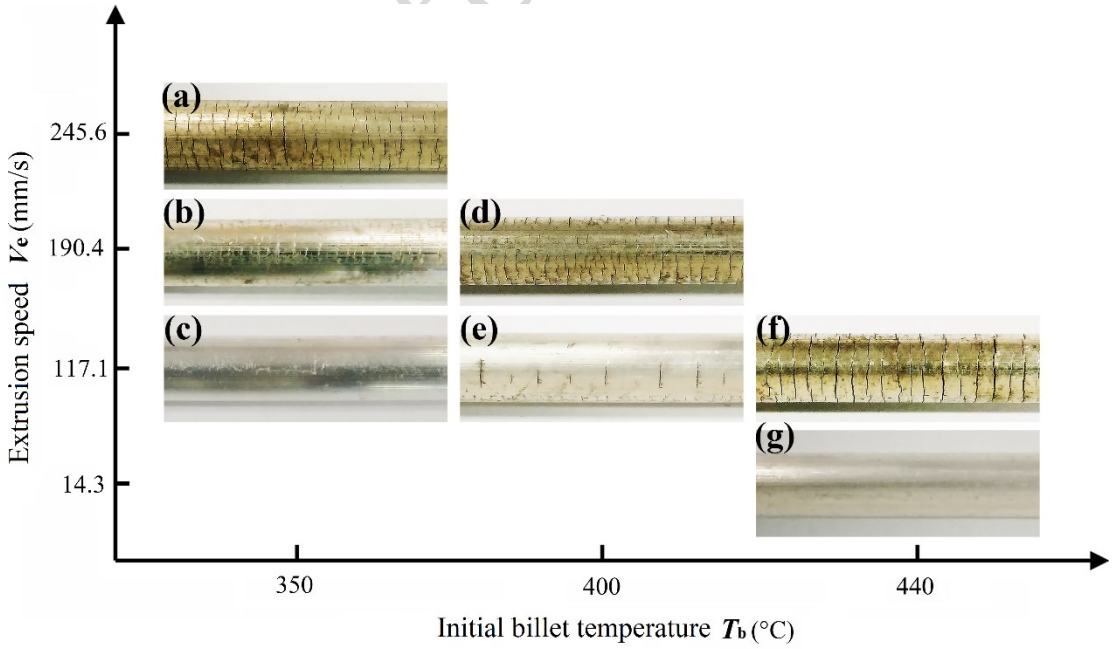

Fig. 13. Magnesium rods extruded at a fixed extrusion ratio of 29.8, different initial billet temperatures and extrusion speeds: (a) 350 °C and 245.6 mm/s; (b) 350 °C and 190.4 mm/s; (c)

350 °C and 117.1 mm/s; (d) 400 °C and 190.4 mm/s; (e) 400 °C and 117.1 mm/s; (f) 440 °C and 117.1mm/s; (g) 440 °C and 14.3 mm/s.

5. Validation of the ELD

Extrusion experiments to produce rectangular and circular tubes through porthole dies were performed to validate the ELD constructed in the present study. Fig. 14 shows the cross sections of the tubes. The width, height and wall thickness of the cross-section of the rectangular tube were 25.4 mm, 12.7 mm and 1.5 mm, respectively. The outer diameter and the wall thickness of the circular tube were 52 mm and 2 mm, respectively. Billets with dimensions of $\phi 75 \times 65$ mm and $\phi 100 \times 65$ mm were used to extrude the rectangular tube and circular tube, respectively. The inner diameters of the container liners to extrude the rectangular tube and circular tube were 80 and 100 mm, respectively, and their extrusion ratios were 47.7 and 25, respectively. In order to verify the predictive capability of the ELD, the parameters employed in tubes extrusion were different from those used in rod extrusion. The initial billet temperatures were 200-450 °C, and the extrusion speeds were 16.2 -125 mm/s. Fig. 15 shows the extruded tubes.

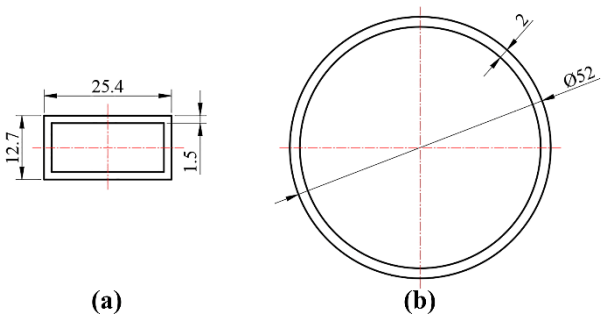

Fig. 14. Cross sections of the rectangular tube (a) and circular tube (b).

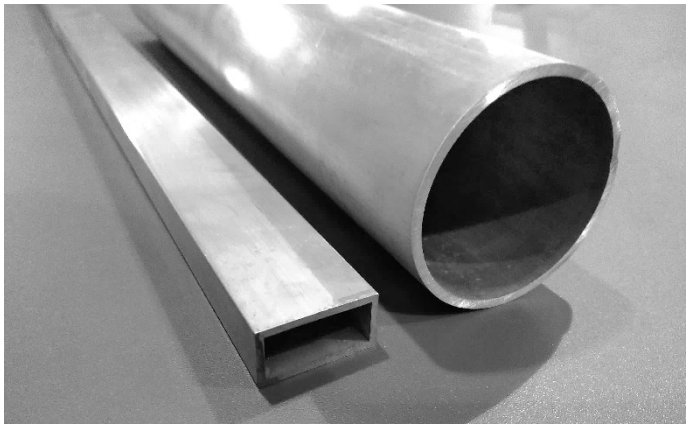

Fig. 15. Extruded magnesium alloy tubes.

The parameters of r, ΔT_{db}, L, D and λ used are listed in Table 5. The calculated equivalent extrusion ratios ($\bar{r}$) for the extrusion of the rectangular tube and circular tube were 78.88 and 46.46, respectively. By intersecting the 3D ELD by planes at constant $\bar{r}$ values of 78.88 and 46.46, the equivalent 2D ELDs for the extrusion of these two tubes were obtained. According to Eqs. (5) and (11)-(15), the equivalent 2D ELDs were converted into real 2D ELDs. In addition, the 2D ELDs constructed by the conventional mathematic models were compared with those constructed by the ANN.

Table 5. Parameters for constructing the 2D ELDs of the rectangular tube and circular tube.

Parameters	r	ΔT_{db} (°C)	L (mm)	D (mm)	λ
Rectangular tube	47.7	40	65	80	3.86
Circular tube	25	40	65	100	5.0

The most widely used empirical models to predict extrusion pressure and temperature changes occurring during extrusion are as follows (Sheppard, 1999):

$$P = \sigma\left(0.171 + 1.86\ln r + \frac{4mL}{\sqrt{3}D}\right) \tag{18}$$

$$\Delta T_1 = \frac{\sigma \ln r}{\sqrt{3}(\rho C)} \tag{19}$$

$$\Delta T_2 = \frac{\sigma}{4\sqrt{3}(\rho C)} \sqrt{\frac{v_R L \rho C}{k}} \tag{20}$$

$$\Delta T_3 = \frac{\sigma}{4\sqrt{3}(\rho C)} \sqrt{\frac{v_e L_D \rho C}{k}} \tag{21}$$

where σ is the flow stress of the deforming material, m the friction coefficient being assumed to have a value of 1, ΔT_1 the temperature rise caused by deformational heat, ΔT_2 the temperature rise caused by the friction between the billet and container, ΔT_3 the temperature increase caused by the friction between the billet and die land, ρ the density of the billet, C the thermal capacity of the billet, k the thermal conductivity of the billet, v_R the ram speed, and L_D the length of die land.

Fig. 16 shows the 2D ELD for the extrusion of the rectangular tube. The solid curves and dash curves represent the extrusion limit curves determined by the ANN and the empirical model, respectively. The safe process window is shown in the green color. The grey area represents the parameters at which the extrusion pressure requirement exceeds the allowable yield strength of the stem. If the parameters in the light red area are selected, hot shortness will occur during the extrusion process.

Fig. 17 shows the rectangular tubes extruded at different conditions corresponding to those shown in the ELD (Fig. 16). The predictions of the ELD constructed by the ANN are in good agreement the experimental results. For example, the tubes extruded at the conditions of a: 300 °C and 95.4 mm/s, b: 400 °C and 47.7 mm/s and c: 450 °C and 16.2 mm/s, located in the safe area (i.e., a, b and c in Fig. 16), all had fine surface

quality (Fig.17a, b and c). Hot shortness indeed occurred at the conditions of d: 350 °C and 95.4 mm/s and e: 450 °C and 47.7 mm/s, as shown in Fig. 17d and e, which was predicted by the ELD (Fig. 16).

Figs. 18 and 19 show the 2D ELD for the extrusion of the circular tube and the corresponding experimental results, respectively. Once again, the experimental results are consistent with the predictions of the ELD. Therefore, the 2D ELD constructed by using the present method is reliable and can provide guidelines for the selection of appropriate extrusion process parameters.

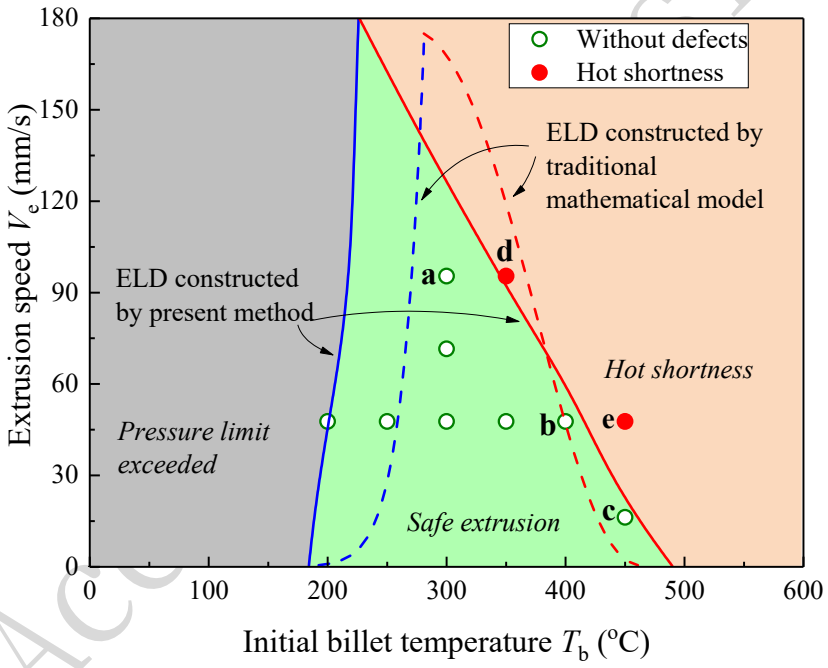

Fig. 16. 2D ELD for the production of the rectangular tubes. The surfaces of the extrudates extruded under the conditions marked by a-e are shown in Fig. 17a-e. (For interpretation of the references to colour in the text, the reader is referred to the web version of this article.)

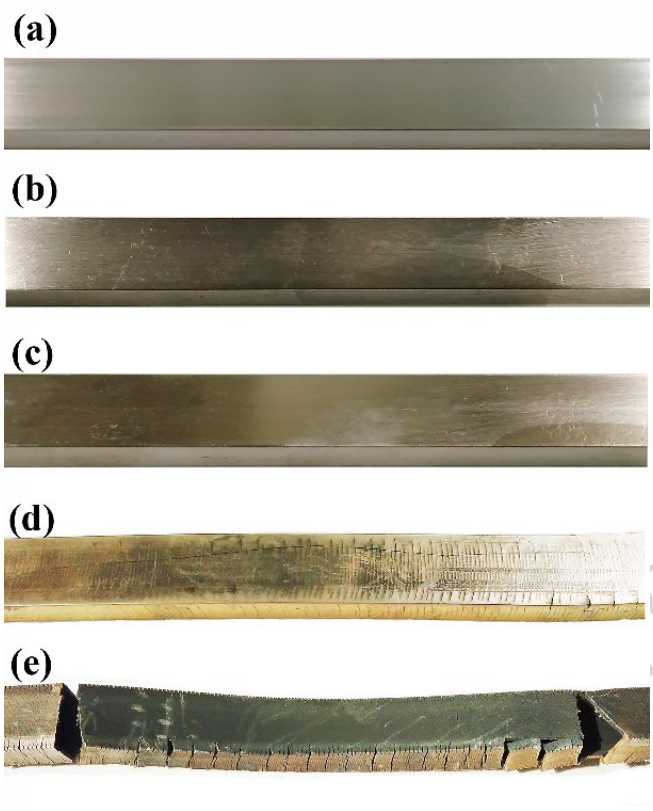

Fig. 17. Rectangular tubes extruded under different conditions: (a) 300 °C and 95.4 mm/s; (b) 400 °C and 47.7 mm/s; (c) 450 °C and 16.2 mm/s; (d) 350 °C and 95.4 mm/s; (e) 450 °C and 47.7 mm/s.

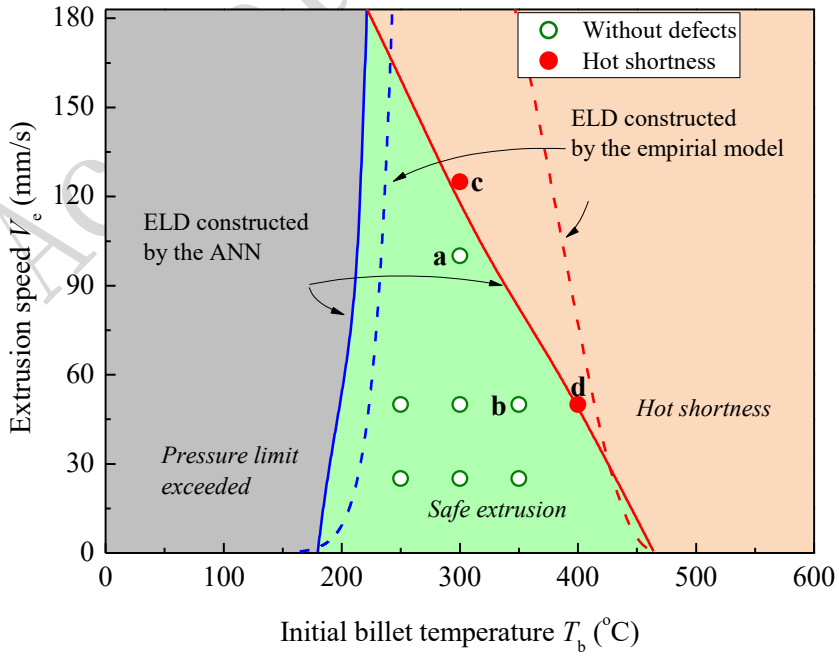

Fig. 18. 2D ELD for the production of the circular tube. The surfaces of the extrudates extruded under the conditions marked by a-d are shown in Fig. 17a-d.

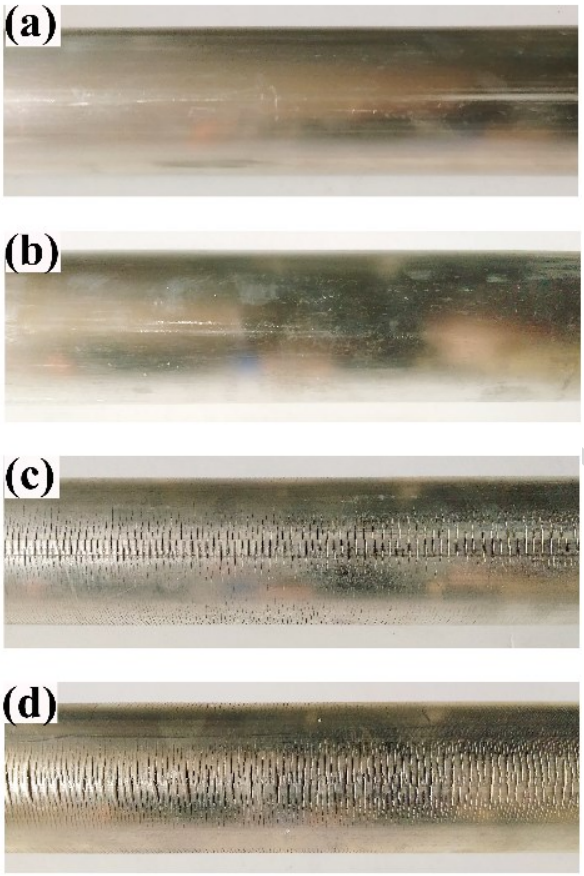

Fig. 19. Circular tubes extruded at different conditions: (a) 300 °C and 100 mm/s; (b) 350 °C and 50 mm/s; (c) 300 °C and 125 mm/s; (d) 400 °C and 50 mm/s.

Furthermore, in comparison with the ELD constructed by the empirical models (the dash lines in Figs. 16 and 18), the ELD developed in the present research makes more reliable predictions for the extrusion of magnesium alloy profiles. This is because the ANN can predict the peak extrusion pressure and extrudate temperature more accurately than the empirical models. Fig. 20 compares the experimentally measured, ANN-predicted and empirical-model-predicted P_{peak} values during extrusion to

produce magnesium alloy rods. Taking the measured values as the reference points, the mean relative errors (MREs) of the P_{peak} values predicted by the ANN and empirical model were 3.34% and 30.44%, respectively. Clearly, the pressures predicted by the empirical model were much higher than those obtained from experiments, while the ANN-predicted pressure values were in good agreement with those obtained from extrusion experiments.

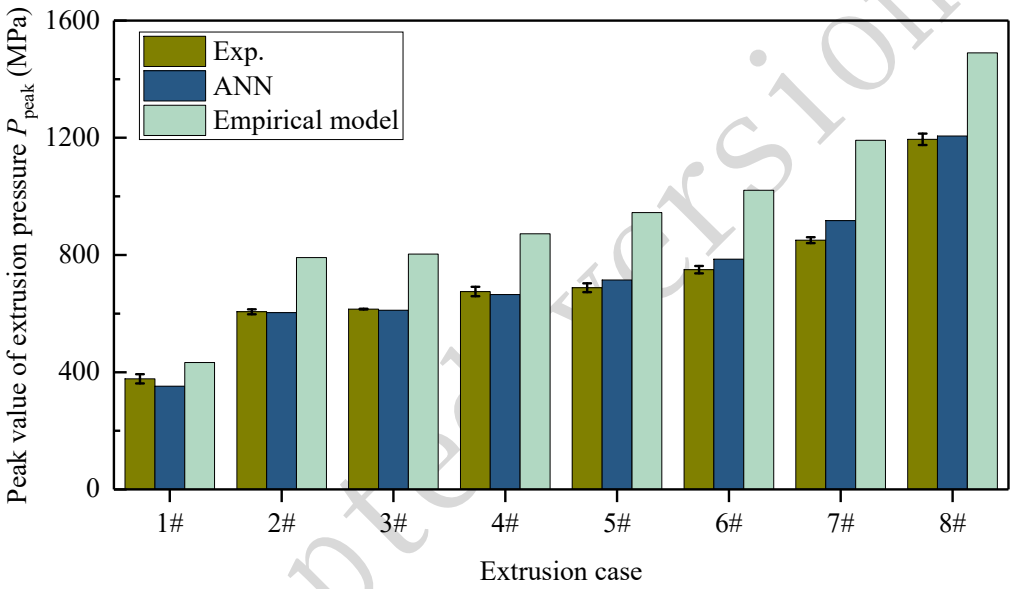

Fig. 20 Peak extrusion pressure values measured during the extrusion experiments and predicted by the ANN and by the empirical model.

6. Conclusions

A 3D ELD for the magnesium alloy Mg-8Al-0.5Zn-0.5RE was constructed in the space of the equivalent extrusion ratio, initial billet temperature and extrusion speed by using the ANN. The following conclusions have been drawn.

(1) After being validated by extrusion experiments, the FE simulations of extrusion of magnesium alloy can be used to provide datasets to be used for training the ANN.

(2) In addition to the main extrusion process parameters, i.e., initial billet temperature, extrusion speed, and extrusion ratio, the influences of billet dimensions, the temperature difference between the die and billet, and extrudate shape on the extrusion results can be integrated into the equivalent process parameters. As a result, the ANN can give high prediction accuracy and generalization performance.

(3) The 3D ELD clearly presents the extrudability of the Mg-8Al-0.5Zn-0.5RE alloy. For the extrusion process to produce magnesium alloy rods, with increasing extrusion ratio from 5 to 105, the maximum extrusion speed decreases from 391 to 259 mm/s.

(4) 2D ELDs for any complex profiles can be obtained through intersecting the 3D ELD. The experimental validation through tube extrusion confirms that the 3D ELD established by the ANN is reliable and can provide guidelines for the selection of appropriate extrusion parameters.

Acknowledgments

The authors (Gang Fang and Shengwen Bai) greatly appreciate the financial support of the National Natural Science Foundation of China (Project No. 51675300).

References

Bai, S., Fang, G., Zhou, J., 2019. Investigation into the extrudability of a new Mg-Al-Zn-RE alloy with large amounts of alloying elements, Metall. Mater. Trans A 50A: 3246-3264, https://link.springer.com/article/10.1007/s11661-019-05242-9 .

Barnett, M., Yao, J., Davies, C., 2003. Extrusion limits for AZ alloys with Al contents< 3%, Proceedings of the 1st International Light Metals Technology Conference 2003, 18-20 September 2003, 333-338, http://dro.deakin.edu.au/view/DU:30005133.

Bauser, M., Sauer, G., Siegert, K., 2006. Extrusion, ASM International, Ohio, 485-486.

Bingöl, S., Ayer, Ö., Altinbalik, T., 2015. Extrusion load prediction of gear-like profile for different die geometries using ANN and FEM with experimental verification, Int. J. Adv. Manuf. Technol. 76, 983-992, https://doi.org/10.1007/s00170-014-6328-z.

Cao, J., Kinsey, B., Solla, S.A., 2000. Consistent and minimal springback using a stepped binder force trajectory and neural network control, J. Eng. Mater. Tech., ASME, 122, 113-118, https://doi.org/10.1115/1.482774.

Carpenter, W.C., Hoffman, M.E., 1997. Selecting the architecture of a class of back-propagation neural networks used as approximators, AI EDAM 11, 33-44, https://doi.org/10.1017/S0890060400001827.

Clade, M., Sheppard, T.,1993. Extrusion limit diagrams containing structural and topological information for AA 6063 aluminium alloy, Mater. Sci. Technol. 9, 313-318, https://doi.org/10.1179/mst.1993.9.4.313.

Ebelechukwu, O.C., Johnson, B.O., Michael, A.I., Fidelis, A.T., 2018. Comparison of some iterative methods of solving nonlinear equations, Int. J. Theor. Appl. Math. 4, 22, https://doi.org/10.11648/j.ijtam.20180402.11.

Haghdadi, N., Zarei-Hanzaki, A., Khalesian, A.R., Abedi, H.R., 2013. Artificial neural network modeling to predict the hot deformation behavior of an A356 aluminum alloy, Mater. Des. 49, 386-391, https://doi.org/10.1016/j.matdes.2012.12.082.

Hornik, K., Stinchcombe, M., White, H., 1989. Multilayer feedforward networks are universal approximators, Neural Netw. 2, 359-366, https://doi.org/10.1016/0893-6080(89)90020-8.

Hsiang, S.H., Kuo, J.L., Yang, F.Y., 2006. Using artificial neural networks to investigate the influence of temperature on hot extrusion of AZ61 magnesium alloy, J. Intell. Manuf. 17, 191-201, https://doi.org/10.1007/s10845-005-6636-0.

Jackson, A., Sheppard, T., 1997. Extrusion limit diagrams: effect of hmogenising conditions and extension to productivity analysis, Mater. Sci. Tech. 13, 61-68, https://doi.org/10.1179/mst.1997.13.1.61.

Kim, J.H., Yeom, J.T., Hong, J.K., Shim, S.Y., Lim, S.G., Park, N.K., 2010. Effect of scandium on the hot extrudability of 7075 aluminum alloy, Met. Mater. Int. 16, 669-677, https://doi.org/10.1007/s12540-010-0823-z.

Li, L., Zhang, H., Zhou, J., Duszczyk, J., Li, G.Y., Zhong, Z.H., 2008. Numerical and experimental study on the extrusion through a porthole die to produce a hollow magnesium profile with longitudinal weld seams, Mater. Des. 29, 1190-1198, https://doi.org/10.1016/j.matdes.2007.05.003.

Li, Y., Bridgwater, J., 2000. Prediction of extrusion pressure using an artificial neural network, Powder Technol. 108, 65-73, https://doi.org/10.1016/S0032-5910(99)00254-5.

Liu, G., Zhou, J., Duszczyk, J., 2008. Process optimization diagram based on FEM simulation for extrusion of AZ31 profile, Trans. Nonferrous Met. Soc. China 18, s247-s251, https://doi.org/10.1016/S1003-6326(10)60211-7.

Liu, G., Zhou, J., Duszczyk, J., 2008. FE analysis of metal flow and weld seam formation in a porthole die during the extrusion of a magnesium alloy into a square tube and the effect of ram speed on weld strength, J. Mater. Process. Technol. 200, 185-198, https://doi.org/10.1016/j.jmatprotec.2007.09.032.

Luo, A.A., Zhang, C., Sachdev, A.K., 2012. Effect of eutectic temperature on the extrudability of magnesium–aluminum alloys, Scripta Mater. 66, 491-494, https://doi.org/10.1016/j.scriptamat.2011.12.025.

Qamar, S.Z., Arif, A.F.M., Sheikh, A.K., 2004. A new definition of shape complexity for metal extrusion, J. Mater. Process. Technol. 155, 1734-1739, https://doi.org/10.1016/j.jmatprotec.2004.04.163.

Ruffini, R., Cao, J., 1998. Using neural network for springback minimization in a channel forming process, No. 980082, SAE Technical Paper, https://doi.org/10.4271/980082.

Sellars, C.M., McTegart, W.J., 1966. On the mechanism of hot deformation, Acta Met. 14, 1136-1138, https://doi.org/10.1016/0001-6160(66)90207-0.

Sheikh-Ahmad, J., Twomey, J., 2007. ANN constitutive model for high strain-rate deformation of Al 7075-T6, J. Mater. Process. Technol. 186, 339-345, https://doi.org/10.1016/j.jmatprotec.2006.11.228.

Sheppard, T., 1999. Extrusion of Aluminum Alloys. Kluwer Academic Publishers, Dordrecht, The Netherlands, 29-51, https://doi.org/10.1007/978-1-4757-3001-2.

Sheppard, T., 1981. Temperature and speed effects in hot extrusion of aluminium alloys, Met. Technol. 8, 130-141, https://doi.org/10.1179/030716981803276009.

Sola, J., Sevilla, J., 1997. Importance of input data normalization for the application of neural networks to complex industrial problems, IEEE T. Nucl. Sci. 44, 1464-1468, https://doi.org/10.1109/23.589532.

Sun, C., Xiang, Y., Liu, G., Zuo, X., Wang, M., Zhang, Q., 2017. Extrusion limit diagram of IN 690 super-alloy tube based on hot processing map, Int. J. Adv. Manuf. Technol. 89, 3419-3428, https://doi.org/10.1007/s00170-016-9271-3.

Tutcher, M., Sheppard, T., 1980. Extrusion limits of Al-5 Mg-0.8 Mn alloy (AA 5456), Met. Technol. 7, 488-493, https://doi.org/10.1179/030716980803286982.

Wang, Y.X., Zeng, X.Q., Ding, W.J., Luo, A.A., Sachdev, A.K., 2007. Development and Validation of Extrusion Limit Diagram for AZ31 and AM30 Magnesium Alloys, MSF. Trans Tech Publ, pp. 327-332, https://doi.org/10.4028/www.scientific.net/MSF.546-549.327.

Yan, J., Pan, Q.L., Li, A.D., Song, B.W., 2017. Flow behavior of Al–6.2 Zn–0.70 Mg–0.30 Mn–0.17 Zr alloy during hot compressive deformation based on Arrhenius and ANN models, Trans. Nonferrous Met. Soc. China 27, 638-647, https://doi.org/10.1016/S1003-6326(17)60071-2.

Zeng, Z., Stanford, N., Davies, C.H.J., Nie, J.F., Birbilis, N., 2019. Magnesium extrusion alloys: a review of developments and prospects, Int. Mater. Rev. 64, 27-62, https://doi.org/10.1080/09506608.2017.1421439.

Table captions

Table 1. Constitutive constants of the magnesium alloy Mg-8Al-0.5Zn-0.5RE.

Table 2. Physical properties of the billet and extrusion tooling.

Table 3. Levels of the parameters used in the FE simulations for preparing ANN training datasets.

Table 4. Variables of the FE simulations for modifying the ELD.

Table 5. Parameters for constructing the 2D ELDs of the rectangular tube and circular tube.

Figure captions

Fig. 1. Schematic of the ELD in the space of extrusion speed (or extrusion ratio) and initial billet temperature.

Fig. 2. Flow chart of the construction of 3D ELD for magnesium alloy.

Fig. 3. Schematic diagram of the experimental setup to produce rods.

Fig. 4. FE axisymmetric model of the extrusion process to produce rods.

Fig. 5 Cross sections of the profiles with different shape factor λ values.

Fig. 6. Comparison between the experimentally measured and simulated extrusion pressures. (a) Extrusion pressure-stroke curves at an extrusion ratio of 29.8, initial billet temperature of 350 °C and extrusion speed of 117.1 mm/s; (b) Linear correlation between the experimental and simulated extrusion pressure values obtained at different extrusion conditions. In the legend, the slop and the correlation coefficient of the fit are given.

Fig. 7. Structure of the ANN used in the present research.

Fig. 8. MSEs of the test dataset calculated by the ANN with different numbers of neurons in the hidden layer.

Fig. 9. Extrusion results predicted by the FE simulations and ANN: (a) normalized peak values of extrusion pressure and (b) normalized peak values of extrudate temperature.

Fig. 10. (a) Regression curve of $\overline{T_b} - T_b$ and (b) influence factor $f_\lambda(\lambda)$.

Fig. 11. 3D ELD for the magnesium alloy.

Fig. 12. 2D ELD for the production of magnesium alloy rods at an extrusion ratio of 29.8. The extrudate surfaces under the extrusion conditions marked by the symbols from a to g are shown in Fig.13.

Fig. 13. Magnesium rods extruded at a fixed extrusion ratio of 29.8, different initial billet temperatures and extrusion speeds: (a) 350 °C and 245.6 mm/s; (b) 350 °C and 190.4 mm/s; (c) 350 °C and 117.1 mm/s; (d) 400 °C and 190.4 mm/s; (e) 400 °C and 117.1 mm/s; (f) 440 °C and 117.1mm/s; (g) 440 °C and 14.3 mm/s.

Fig. 14. Cross sections of the rectangular tube (a) and circular tube (b).

Fig. 15. Extruded magnesium alloy tubes.

Fig. 16. 2D ELD for the production of the rectangular tubes. The surfaces of the extrudates extruded under the conditions marked by a-e are shown in Fig. 17a-e. (For interpretation of the references to colour in the text, the reader is referred to the web version of this article.)

Fig. 17. Rectangular tubes extruded under different conditions: (a) 300 °C and 95.4 mm/s; (b) 400 °C and 47.7 mm/s; (c) 450 °C and 16.2 mm/s; (d) 350 °C and 95.4 mm/s; (e) 450 °C and 47.7 mm/s.

Fig. 18. 2D ELD for the production of the circular tube. The surfaces of the extrudates extruded under the conditions marked by a-d are shown in Fig. 17a-d.

Fig. 19. Circular tubes extruded at different conditions: (a) 300 °C and 100 mm/s; (b) 350 °C and 50 mm/s; (c) 300 °C and 125 mm/s; (d) 400 °C and 50 mm/s.

Fig. 20 Peak extrusion pressure values measured during the extrusion experiments and predicted by the ANN and by the empirical model.